Planetary and Space Science 121 (2016) 27–35

Contents lists available at ScienceDirect

Planetary and Space Science

journal homepage: www.elsevier.com/locate/pss

Asteroid Impact & Deflection Assessment mission: Kinetic impactor

A.F. Cheng [a,*], P. Michel [b], M. Jutzi [c], A.S. Rivkin [a], A. Stickle [a], O. Barnouin [a], C. Ernst [a], J. Atchison [a], P. Pravec [d], D.C. Richardson [e], AIDA team, AIM team

[a] The Johns Hopkins University Applied Physics Laboratory, Laurel, Maryland
[b] Lagrange Laboratory, University of Nice, CNRS, Côte d'Azur Observatory, France
[c] University of Bern, Switzerland
[d] Ondrejov Observatory, Czech Republic
[e] University of Maryland, USA

ARTICLE INFO

Article history:
Received 17 August 2015
Received in revised form
2 November 2015
Accepted 13 December 2015
Available online 4 January 2016

Keywords:
Planetary defense
Near-Earth asteroids
Asteroid impact hazards
Kinetic impactor
Binary asteroids

ABSTRACT

The Asteroid Impact & Deflection Assessment (AIDA) mission will be the first space experiment to demonstrate asteroid impact hazard mitigation by using a kinetic impactor to deflect an asteroid. AIDA is an international cooperation, consisting of two mission elements: the NASA Double Asteroid Redirection Test (DART) mission and the ESA Asteroid Impact Mission (AIM) rendezvous mission. The primary goals of AIDA are (i) to test our ability to perform a spacecraft impact on a potentially hazardous near-Earth asteroid and (ii) to measure and characterize the deflection caused by the impact. The AIDA target will be the binary near-Earth asteroid (65803) Didymos, with the deflection experiment to occur in late September, 2022. The DART impact on the secondary member of the binary at ~7 km/s is expected to alter the binary orbit period by about 4 minutes, assuming a simple transfer of momentum to the target, and this period change will be measured by Earth-based observatories. The AIM spacecraft will characterize the asteroid target and monitor results of the impact in situ at Didymos. The DART mission is a full-scale kinetic impact to deflect a 150 m diameter asteroid, with known impactor conditions and with target physical properties characterized by the AIM mission. Predictions for the momentum transfer efficiency of kinetic impacts are given for several possible target types of different porosities, using Housen and Holsapple (2011) crater scaling model for impact ejecta mass and velocity distributions. Results are compared to numerical simulation results using the Smoothed Particle Hydrodynamics code of Jutzi and Michel (2014) with good agreement. The model also predicts that the ejecta from the DART impact may make Didymos into an active asteroid, forming an ejecta coma that may be observable from Earth-based telescopes. The measurements from AIDA of the momentum transfer from the DART impact, the crater size and morphology, and the evolution of an ejecta coma will substantially advance understanding of impact processes on asteroids.

© 2015 Elsevier Ltd. All rights reserved.

1. Introduction

On February 15, 2013, the small, 30 m asteroid 367943 Duende (2012 DA14) made an exceptionally close approach to Earth and passed inside the geosynchronous orbit radius, after having been discovered in February 2012. However, February 15, 2013 is remembered for an entirely different reason, as another, still smaller asteroid unexpectedly hit the Earth near Chelyabinsk, Russia on that same day without warning. The Chelyabinsk impact (Popova et al., 2013; Brown et al., 2013), of a roughly 20 m object, released 500 kton TNT of energy, injured over 1500 people, and caused extensive property damage.

The Chelyabinsk impact served as a dramatic reminder of the asteroid impact hazard and re-emphasized the importance of discovering hazardous asteroids and learning how to mitigate them. NASA was tasked in 1994 with identifying potentially hazardous asteroids greater than 1 km (0.62 miles) in diameter, and the NASA Authorization Act of 2005 required the agency to detect at least 90% of Near-Earth Objects (NEOs, small bodies with perihelia ≤ 1.3 AU) of 140 m or larger. Following an OSTP letter to the US Congress (Holdren, 2010), NASA has undertaken the lead in the analysis and simulation of asteroid mitigation and deflection, as well as the assessment of applicable technologies. In Europe, the NEOShield Project has been funded by the European Commission (EC) in its FP7 program since 2012 (Harris et al., 2013), to analyze asteroid mitigation options and address the scientific and technical issues. A continuation of this project, called NEOShield 2, funded by the EC program Horizon 2020 and focused on NEO

* Corresponding author.
E-mail address: andrew.cheng@jhuapl.edu (A.F. Cheng).

http://dx.doi.org/10.1016/j.pss.2015.12.004
0032-0633/© 2015 Elsevier Ltd. All rights reserved.

physical characterization as well as space mission technologies started in March 2015 for 2.5 years.

There are many unknowns with respect to how an incoming NEO might best be deflected (Ahrens and Harris, 1994; Harris et al., 2013; Michel, 2013). Strategies to deflect an asteroid include impacting it with a spacecraft (a kinetic impactor), pulling it with the gravity of a massive spacecraft (a gravity tractor), using the blast of a nearby nuclear explosion, and modifying the surface or causing ablation by various means including lasers or particle beams. The impulsive methods to change an asteroid's orbit, kinetic impact and blast deflection, achieve immediate effects, whereas the non-impulsive methods may require years of operation to accumulate a sufficient deflection, and hence they require the hazardous object to be discovered more years in advance of its threatened collision with Earth.

However, none of these strategies for asteroid hazard mitigation has ever been tested on a NEO, and deflection of a NEO has never been demonstrated. The unknowns, in assessing strategies for deflecting an incoming asteroid, begin with unknowns concerning the threatening object itself: how large is it, what are its physical properties, how certain is the NEO to hit the Earth, and where will it hit. Also, if energy and momentum are applied to the NEO, impulsively or non-impulsively, in various ways, how much deflection will result, and over how much time? The physical properties of the NEO are vitally important to address the latter questions (Michel, 2013). Questions of costs and risks – technical, programmatic, and political – are critical as well but are not addressed here.

This paper focuses on the kinetic impactor strategy and specifically on a first demonstration of asteroid deflection by kinetic impact. The kinetic impactor approach has attracted interest owing to its relevance to asteroid collisions and cratering processes, and the issue of momentum transfer efficiency (what is the ratio β of momentum transferred to the momentum incident?) has been the subject of analytical, experimental, and computational studies (Ahrens and Harris, 1994; Holsapple and Housen, 2012; Cheng, 2013; Jutzi and Michel, 2014; Cheng et al., 2015). The Don Quijote mission, proposed by ESA as an asteroid deflection experiment by kinetic impactor (Carnelli et al., 2006), was the subject of Phase A industry studies but did not reach implementation phase. The Deep Impact spacecraft impacted comet 9P/Tempel 1 in July, 2005, without causing any measurable deflection or intending to (A'Hearn et al., 2005).

When a kinetic impactor of mass m strikes a target at speed U, the impulse p transferred to the target exceeds mU because of momentum p_{ej} carried away by impact ejecta released back towards the incident direction, and the momentum transfer efficiency β is defined by

$$p = \beta mU = p_{ej} + mU \quad (1)$$

where $\beta > 1$ unless there are ejecta released in the forward direction (a possible effect, not considered here). In this paper, we will discuss expectations for β based on crater scaling laws and on numerical computations.

This paper and its companion paper (Michel et al., submitted for publication) present science goals and objectives, payloads, measurements, and expected results of the Asteroid Impact & Deflection Assessment (AIDA) mission, which is an international collaboration between NASA and ESA (Cheng et al., 2015). AIDA will make the first demonstration of asteroid deflection by kinetic impact. In this paper, we describe the science of the kinetic impactor mission, which is one of the two independent but mutually supporting mission elements of AIDA. The NASA Double Asteroid Redirection Test (DART) is the asteroid kinetic impactor mission, and the ESA Asteroid Impact Mission (AIM) is the characterization spacecraft, for the joint AIDA mission.

The AIDA target will be the binary near-Earth asteroid (65803) Didymos, with the deflection experiment to occur in late September or October, 2022. The DART impact on the secondary member of the binary at ~7 km/s will alter the binary orbit period. The change in the period will be measured to within 10% by Earth-based observations. Hence DART will determine directly the efficiency of impact kinetic energy transfer to the orbital energy, even without measurements from AIM. The impactor autonomously targets the asteroid centroid, to maximize the likelihood of successful kinetic impact. The AIM spacecraft will rendezvous with Didymos in advance of the DART impact to characterize the asteroid target and determine its key physical properties (Michel et al., submitted for publication). AIM will monitor results of the DART impact in situ and will make more precise measurements of the orbital speed change Δv induced by the kinetic impact and hence the momentum transfer, as well as another physical characterization of the target after the impact. Additional results of the DART impact, like the impact crater and the long-term evolution of impact ejecta, will be studied in detail by the AIM mission.

The combined mission AIDA will make the first measurement of momentum transfer efficiency from hypervelocity kinetic impact at full scale on an asteroid, where impact conditions of the projectile are known, and physical properties and internal structures of the target asteroid are also characterized. The two mission components of AIDA, namely DART and AIM, are each independently valuable, but together provide a greatly increased knowledge return. Supporting Earth-based optical and radar observations and numerical simulation studies will be an integral part of the DART mission.

Here we present the objectives, requirements and design of the DART mission as well as analyses of predicted outcomes from the kinetic impact including estimates of momentum transfer efficiency β from the DART impact on the Didymos secondary. The momentum transfer has been estimated using hypervelocity impact models based on crater scaling relations (Housen and Holsapple, 2011) and numerical simulations (Jutzi and Michel, 2014). We outline a simple method similar to that of Holsapple and Housen (2012) to estimate the momentum transfer efficiency using crater scaling law relations for a variety of target conditions and performing numerical integrations over ejecta mass versus velocity distributions.

The present model of momentum transfer in a kinetic impact is improved from previous work (Holsapple and Housen, 2012; Cheng et al., 2015) by incorporating more realistic ejecta velocity distributions fitted to laboratory experiments (Housen and Holsapple, 2011) instead of truncated power laws. The more accurate mass versus ejecta velocity distributions yield better estimates of momentum transfer efficiency and moreover enable direct comparisons with numerical simulation results (e.g. Jutzi and Michel, 2014). The present model also estimates the observability of ejecta from the kinetic impact, including the possibility that ejecta may form a dust coma observable by ground-based telescopes.

2. Objectives and requirements

The main objectives of the DART mission, which includes the spacecraft kinetic impact and an Earth-based observing campaign, are to:

- Perform a full-scale demonstration of the spacecraft kinetic impact technique for deflection of an asteroid, by targeting an object large enough to qualify as a Potentially Hazardous Asteroid (that is, larger than 100 m), which is large enough if an impact occurs to cause major damage on regional scales larger than a metropolitan area.

- Measure the resulting asteroid deflection, by targeting the secondary member of a binary NEO and measuring the period change of the binary orbit.
- Understand the hypervelocity collision effects on an asteroid, including the long-term dynamics of impact ejecta; validate models for momentum transfer in asteroid impacts, inferring physical properties of the asteroid surface and sub-surface.

DART is targeted to impact the smaller secondary component of the binary system [65803] Didymos, which is already well characterized by radar and optical instruments (Pravec et al., 2003; Scheirich and Pravec, 2009). The impact of the >300 kg DART spacecraft at 6.67–7.38 km/s (depending on launch date) will produce a speed change on the order of 0.4 mm/s (assuming $\beta=1$, i.e. no contribution of impact ejecta), which leads to a significant change in the mutual orbit of these two objects, but only a minimal change in the heliocentric orbit of the system. This is because the target's speed change from the impact is significant compared to its orbital speed $\sim$17 cm/s, although it is quite small compared to the heliocentric orbit speed $\sim$23 km/s. Thus the change in the binary orbit of Didymos is relatively easy to measure compared with the change in the heliocentric orbit.

The DART mission will use ground-based observations to make the required measurements of the orbital deflection, by measuring the orbital period change of the binary asteroid. The DART impact is expected to change the 11.92 h Didymos orbit period (Michel et al. 2015a, submitted for publication) by at least several minutes, and this change can be determined to 10% accuracy within months of observations. Didymos is chosen as the DART target because it is an eclipsing binary, which enables accurate determination of small period changes by ground-based optical light curve measurements. In an eclipsing binary, the two objects pass in front of each other (occultations), or one object creates solar eclipses seen by the other, so there are sharp features in the light curves that can be timed accurately. In addition, Didymos makes a close approach to Earth in October, 2022 which is exceptionally favorable for intercept and rendezvous missions as well as for Earth-based observing (Cheng et al., 2015).

The DART payload consists of a high-resolution visible imager to support the primary mission objective of impacting the target body through its center. The DART imager is required to support optical navigation on approach and autonomous navigation in the terminal phase. The imager is derived from the New Horizons LORRI instrument (Cheng et al., 2008), which used a 20 cm aperture Ritchey–Chretien telescope to obtain images at 1″ per pixel. The DART imager will determine the impact point within 1% of the target diameter, and it will characterize the pre-impact surface morphology and geology of the target secondary asteroid to <20 cm/px.

3. DART mission design

DART can be launched on a small launch vehicle for the baseline mission in December, 2020 to impact the Didymos secondary in September, 2022. There are multiple launch opportunities for the 2022 Didymos close approach to Earth, providing program flexibility. The December 20, 2021 launch for DART shown by Cheng et al. (2015) is the back-up launch opportunity.

The baseline mission design (opening of launch window) is shown in Fig. 1 and Table 1. The DART trajectory was designed for minimum launch energy and favorable arrival conditions. The arrival relative velocity should lie mostly in the binary orbital plane to maximize the orbital period change, and the solar phase angle should be minimized for optimum illumination.

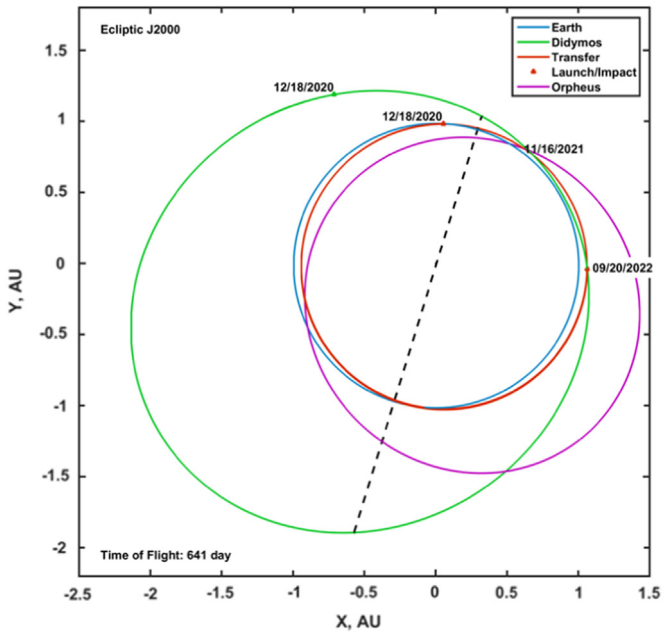

Fig. 1. DART launches December 18, 2020 and intercepts the secondary member of 65803 Didymos on September 20, 2022. Dashed line is the Didymos line-of-nodes. A flyby of 3361 Orpheus occurs on November 16, 2021.

Table 1
Baseline DART trajectory.

Launch date	December 18, 2020
Launch C_3	6.0 km^2/s^2
Arrival relative speed	7.03 km/s
Time of flight	640 days
Maximum earth distance	0.21 AU
Solar distance	0.95–1.06 AU
Earth distance at impact	0.087 AU
Incoming solar phase angle	44°
Impact angle, relative to orbit plane	27.5°

The DART trajectory remains near 1 AU from the Sun and has a maximum Earth distance <0.21 AU. At the opening of the launch window, the impact speed on Didymos is 7.03 km/s, but it is at least 6.67 km/s over the entire window. The approach direction is at an angle of 27.5° to the orbital plane of Didymos. The approach solar phase angle is favorable for imaging of the target at 44°. A mono-propellant propulsion system provides $\sim$250 m/s for trajectory corrections, terminal guidance, and attitude control.

The DART launch is close to the time of the AIM launch in late October, 2020 for approximate alignment of the two development programs. AIM arrival at Didymos is in late May–early June, 2022, allowing more than 3 months for characterization of the Didymos system prior to the DART impact. The DART time of flight is less than two years to impact the Didymos secondary on September 20, 2022. A key feature of the DART mission design is that an opportunity exists to execute an $\sim$8 km/s flyby of the NEO 3361 Orpheus in November, 2021, about 11 months after launch and about 10 months before the Didymos encounter. Science return is maximized if the AIM rendezvous spacecraft is at Didymos before, during, and after impact, but AIDA mission goals can be met even if the rendezvous occurs after the impact (Michel et al., submitted for publication).

3.1. Target asteroid

The target asteroid for DART is the smaller component of the binary near-Earth asteroid (65803) Didymos. Binary systems are of

particular interest and comprise roughly 15% of the NEO population (Margot et al., 2002; Pravec et al., 2006). In addition to the planetary defense applications, AIDA will be the first mission to study a binary NEO.

Based upon optical and radar observations, the satellite of Didymos orbits the primary with a period of 11.92 $(+0.004/-0.006)$ hours, a best-fit semi-major axis of 1.18 $(+0.04/-0.02)$ km, and a low-eccentricity orbit, $e<0.03$ (Michel et al., 2015a, submitted for publication). The primary has a diameter of 775 ± 80 m, the secondary about 160 m. The system mass is inferred from Kepler's law to be 5.28×10^{11} kg, with the density of the primary estimated as 2.146 ($\pm30\%$) g/cm^3. This model for Didymos adopted the retrograde pole solution (eclipticlongitude, latitude) $=(310^\circ,-84^\circ)$ which updates the Pole 2 solution of Scheirich and Pravec (2009); see Michel et al. (submitted for publication).

Ground-based reflectance spectroscopy of Didymos shows it to be a member of the "S complex" of asteroids, the most common compositional group of NEOs. This group includes the spacecraft targets (433) Eros and (25143) Itokawa and is associated with the common ordinary chondrite meteorites. The choice of an S-complex asteroid ensures that the mitigation demonstration will be applicable to a large fraction of the likeliest potential Earth impactors.

4. Deflection effects

The key objective of the AIDA mission is to measure the change in the orbit velocity of the Didymos secondary as a result of kinetic impact by the >300 kg DART spacecraft at ~7 km/s. The changes in the binary orbit elements are estimated below.

Current theories of asteroid satellite formation predict satellites should have similar or smaller densities than the primaries (Richardson and Walsh, 2006; Walsh et al., 2012). From the system mass 5.28×10^{11} kg and the diameter ratio (Scheirich and Pravec, 2009), the calculated mass of the secondary is 4.8×10^9 kg. For the lowest momentum transfer efficiency $\beta=1$, where the incident momentum is just transferred to the target, linear momentum conservation gives a target Δv of ~0.4 mm/s. It is expected that the momentum transfer efficiency to the target will be $\beta>1$, because of crater ejecta released backwards in the incident direction. The momentum carried off by crater ejecta can lead to $\beta>3$ (Holsapple and Housen, 2012).

If, for simplicity, the binary orbit before the kinetic impact is assumed to be circular, since zero eccentricity is consistent with current orbit knowledge (Scheirich and Pravec, 2009), then only the component of Δv along the orbit velocity component causes an orbital period change. The changes in the period, eccentricity, and inclination of the binary orbit depend on the orbit phase at which the impact occurs (Fig. 2). The period change vanishes if the impact occurs at either of two orbit phases where the incident momentum is orthogonal to the orbital velocity; one of which is chosen as the zero of true anomaly in Fig. 2. DART will target a true anomaly near 90°, where the period change and the eccentricity change are both maximized. The inclination change is almost, but not exactly, independent of the impact true anomaly.

With the DART impact at 27.5° out of the binary orbit plane, the velocity change component along the orbit velocity is 0.35 mm/s for $\beta=1$, producing a maximal period change of 4.4 min at 90° true anomaly. The eccentricity change is also maximal there, leading to $e=0.004$, whereas the inclination change is nearly independent of the impact true anomaly at $i=3.7'$. DART will target an impact true anomaly near 90°, which is preferred to targeting near 270° because of lighting conditions (in the selected encounter geometry, the night side of the target is illuminated by reflected light from the binary companion).

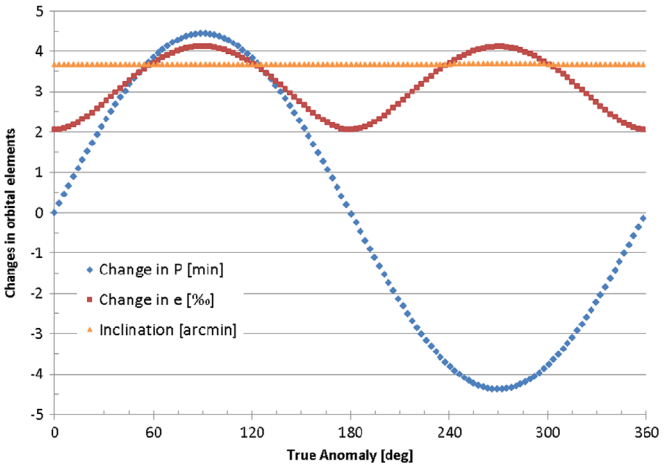

Fig. 2. Changes in binary orbit period, eccentricity, and inclination after DART impact at 27.5° out of the orbit plane, assuming a total velocity change of 0.4 mm/s and an initial circular orbit. DART will target a true anomaly ~90°.

The binary period change resulting from the DART kinetic impact will cause a shift in timing of mutual events observed from the Didymos system. The mutual events observed from Didymos include Earth occultations, where one member of the binary occults the other as seen from Earth, as well as solar eclipses, where one member casts a shadow on the other (Scheirich and Pravec, 2009). The DART mission includes a ground-based observing program to measure mutual event timing from Didymos light curves. With a change ΔP in the binary period P, a shift in the orbital phase of a given mutual event occurs that accumulates linearly with time. The total shift in orbital phase amounts to $2\pi/10$ (roughly the full width of a mutual event) within 30 days for

$$\frac{\Delta P}{P}>0.17\%$$

A period change of 4.4 min would amount to $\Delta P/P=0.6\%$ and is expected to be measurable within a few days with ground-based photometric observations.

4.1. Momentum transfer from kinetic impact

We consider a spherical impactor of mass m and velocity U at normal incidence on a spherical target, with the impact occurring along the centerline. We use crater scaling relations and assume ballistic trajectories to find the momentum carried off to infinity by ejecta. The scaling relations take the forms given by Housen and Holsapple (2011), where the total mass of ejecta is expressed in terms of the crater radius R, non-dimensionalized by target density ρ and impactor mass m. This combination is expressed in terms of the conventional dimensionless scaling parameters $\pi_2=\frac{ga}{U^2}$ and $\pi_3=\frac{Y}{\rho U^2}$ in the gravity- or strength-dominated impact cases, respectively. Here π_2 is the gravity-scaled size, with g the target surface gravity and a the projectile radius; and π_3 is the strength parameter (the ratio of material strength and inertial stresses) with target impact strength Y and target density ρ. In the gravity-dominated case, the crater radius R is given by

$$R\left(\frac{\rho}{m}\right)^{1/3}=H_1\left(\frac{\rho}{\delta}\right)^{\frac{2+\mu-6\nu}{3(2+\mu)}}\left(\frac{ga}{U^2}\right)^{-\frac{\mu}{2+\mu}}\ \text{(gravity)} \tag{2}$$

The strength scaling case applies to kinetic impacts at the scale of the DART impact (Housen and Holsapple, 2011) for plausible

Table 2
Impact ejecta scaling parameters from Housen and Holsapple (2011).

Target[a]	Poro-sity (%)	μ	C_1	k	H_2	p	a (mm)	U (m/s)	δ (kg/m3)	ρ (kg/m3)	Y (MPa)
Basalt C2	~0	0.55	1.5	0.3	1.1	0.5	1.6	6200	2700	3000	30
WCB C3	20	0.46	0.18	0.3	0.38	0.3	3.6	1860	2700	2600	0.45
SFA C7	45	0.4	0.55	0.3	0.4	0.3	7	1900	930	1500	0.004
PS C8	60	0.35	0.6	0.32	0.81	0.2	8.7	1800	940	1200	0.002

[a] WCB=weakly cemented basalt; SFA = sand/fly ash; PS=perlite/sand; C2, C3, C7 and C8 are labels used by Housen and Holsapple (2011); in all cases, $\upsilon = 0.4$, $n_1 = 1.2$, $n_2 = 1$.

values of the target strength. In this case the crater radius R is

$$R\left(\frac{\rho}{m}\right)^{1/3} = H_2\left(\frac{\rho}{\delta}\right)^{(1-3\nu)/3}\left(\frac{Y}{\rho U^2}\right)^{-\mu/2} \quad \text{(strength)} \tag{3}$$

The dimensionless scaling parameter μ depends on target properties and lies in the range $1/3 < \mu < 2/3$, where $\mu = 1/3$ is the momentum scaling limit, and $\mu = 2/3$ is the energy scaling limit. The non-dimensional parameter ν enters via the ratio of target to projectile densities $\frac{\rho}{\delta}$ and is about 0.4 for any target material. The normalization of crater size (and thus total ejecta mass) is given by H_1 or H_2 (only H_2 for strength-dominated impacts is used here). Empirical values for these parameters, based on fitting to ejecta distributions from laboratory experiments, are shown in Table 2 for the four strength-dominated target material cases given by Housen and Holsapple (2011). These cases are labeled C2, C3, C7 and C8 corresponding to the labels used by Housen and Holsapple (2011).

The speed of ejecta v, non-dimensionalized by the incident velocity U, that are released at radial distance x from the central point of impact is

$$\frac{v}{U} = C_1\left[\frac{x}{a}\left(\frac{\rho}{\delta}\right)^{\nu}\right]^{-\frac{1}{\mu}}\left(1-\frac{x}{n_2 R}\right)^{p} \tag{4}$$

The mass M ejected from within x, which is also the mass ejected above the corresponding speed according to Eq. (4), is

$$\frac{M}{m} = \frac{3k}{4\pi}\frac{\rho}{\delta}\left[\left(\frac{x}{a}\right)^3 - {n_1}^3\right] \tag{5}$$

This model for the ejecta velocity distribution is not a power law. Eqs. (4) and (5) reproduce the velocity distributions seen in laboratory impact experiments: at high ejecta velocities, there is an ejecta mass cutoff at small $x = n_1 a$, and at low ejecta velocities, there is a velocity cutoff at large $x = n_2 R$. The parameter C_1 normalizes ejecta velocities, and the parameter k normalizes ejecta mass (or equivalently, crater depth versus diameter) accounting for compaction and uplift.

Among the four target cases shown in Table 2, the parameter k is nearly the same for all of them, but the parameter C_1 varies over a factor of 8.3 between the strong, non-porous basalt case and the moderately porous, weakly-cemented basalt case. These C_1 values directly influence the momentum transfer efficiency β, where the basalt case will give the largest β value, while the WCB case will give the smallest value, with the other porous cases giving intermediate values.

The mass dM ejected in radial distance range dx is

$$dM = \frac{9km}{4\pi}\frac{\rho}{\delta}\left(\frac{x}{a}\right)^2\frac{dx}{a} \tag{6}$$

This mass carries off to infinity a momentum $v_{inf}\cos\theta dM$. Here v_{inf} is the speed at infinity, where $v_{inf} = 0$ below the escape velocity; and $\cos\theta$ gives the component of the asymptotic velocity along the incidence direction, assuming ejection at 45° to the incidence direction onto ballistic trajectories from a spherical target (see Fig. 3).

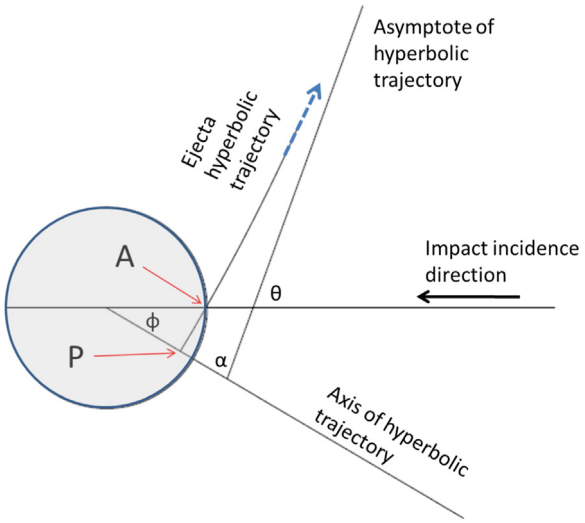

Fig. 3. Ballistic trajectories of ejecta launched at 45° from impact point A; if hyperbolic trajectory were extended back into body, the periapse would be at point P. The true anomaly at ejecta launch is φ and the angle of the asymptote is α.

The total momentum carried to infinity by impact ejecta is given by integration over $w = \frac{x}{a}$

$$p_{ej} = \frac{9km}{4\pi}\frac{\rho}{\delta}\int_{n_1}^{\frac{n_2 R}{a}} dw\, w^2 v_{inf}\,\cos\,\theta \tag{7}$$

Defining $u = \frac{v}{v_{esc}}$ we have for the hyperbolic ejecta trajectory of eccentricity e (see Fig. 3)

$$\cos\theta = \sin\varphi\sin\alpha - \cos\varphi\cos\alpha$$

$$\frac{v_{inf}}{v_{esc}} = \sqrt{u^2-1}$$

$$e\,\cos\,\varphi = u^2 - 1$$

$$e = \left(1+2u^2\left(u^2-1\right)\right)^{1/2} = \frac{1}{\cos\,\alpha}$$

The integral over w is evaluated by Gaussian quadrature, where (4) is used to relate u to w.

The momentum transfer efficiency is then given by

$$\beta - 1 = \frac{p_{ej}}{mU} \tag{8}$$

This model for the momentum transfer efficiency is improved over previous work (Holsapple and Housen, 2012; Cheng, 2013: Cheng et al., 2015), by using the ejecta velocity distributions of Housen and Holsapple (2011) instead of approximate power law distributions. The present model also accounts for the ballistic slowing and bending of ejecta. However, it does not account for the target's being in a binary system, as will be discussed below.

In the present model, the dependence of $\beta - 1$ on the incident velocity U is no longer a pure power law, but U enters primarily through the upper limit of the integral in Eq. (7), where the crater radius R appears and is related to U by Eq. (3). With the present model, the incident velocity dependence is nevertheless similar to

that found in previous models (Holsapple and Housen, 2012; Jutzi and Michel, 2014; Cheng et al., 2015), in which there is a power law dependence on incident velocity, namely $\beta-1 \propto U^{3\mu-1}$.

This is demonstrated using an approximation to (7) derived by observing that the dominant contribution to $\beta-1$ comes from the lower velocity ejecta as found previously (Holsapple and Housen 2012). For $x < 0.74 n_2 R$, we approximate (4) with the power law

$$\frac{v}{U} \cong C_1 \left[\frac{x}{a} \left(\frac{\rho}{\delta} \right)^{\nu} \right]^{-\frac{1}{\mu}}$$

and use $v_{inf} \cos\theta \cong \frac{v}{\sqrt{2}}$ to obtain

$$\beta - 1 \cong \frac{9kC_1}{4\pi\sqrt{2}} \left(\frac{\rho}{\delta} \right)^{\frac{(\mu-\nu)}{\mu}} \frac{\mu}{3\mu-1} \left\{ \left(0.74 n_2 \frac{R}{a} \right)^{\frac{(3\mu-1)}{\mu}} - n_1^{\frac{(3\mu-1)}{\mu}} \right\} \tag{9}$$

The coefficient 0.74 comes from fitting (9) to numerical integrations of (7). If we now neglect the second term in the curly bracket compared to the first, and we use (3), we find

$$\beta - 1 \propto (kC_1) \left(\frac{\rho}{\delta} \right)^{1-3\nu} \left(\frac{\mu}{3\mu-1} \right) H_2^{\frac{(3\mu-1)}{\mu}} \left(\frac{U}{\sqrt{\frac{Y}{\rho}}} \right)^{3\mu-1} \tag{10}$$

Hence in this approximation, the power law dependence on incident velocity is recovered as is a power law dependence on the strength Y. Also, the importance of the target-dependent empirical parameters of Table 2 becomes clear. With the value $\nu = 0.4$ adopted for all target cases, the $\beta-1$ increases slowly with increased projectile density. The factor $f = \mu/(3\mu-1)$ is a monotone decreasing function, decreasing from $f = 2$ for $\mu = 0.4$, to $f = 0.75$ for $\mu = 0.6$, but target cases with lower μ also tend to have lower C_1. The parameters k and n_2 exhibit little or no variation between cases. The n_1 term in (9), which is neglected to obtain the power law form (10), can be important for cases with low μ approaching 1/3, as for case PS C8.

An important property of the scaling law model is that the momentum transfer efficiency β does not depend on the mass of the impactor if all else is held constant: if there are impacts of more massive and less massive projectiles of the same density, at the same velocity, into the same target material, the β values are the same. This property applies as long as the impacts are strength dominated, according to (7) and also to the approximation (9), and it is important for extensibility of the DART demonstration to future kinetic impactor mitigations.

Also noteworthy is that the parameter μ may become close to (but greater than) 1/3 for highly porous target materials. In this case, $\beta-1$ still depends on the target parameters kC_1, but the dependences on H_2 and more importantly on the incident velocity U and on strength Y become very weak.

The magnitude of β from a kinetic impact further depends on impact angle and on target structure (Gault and Wedekind, 1978; Cintala et al., 1999; Yamamoto et al., 2009), and hence may depend on the moment arm of the incident momentum relative to the center of the mass. These effects will be explored with numerical simulations in future work.

4.2. Applications to DART impact

Table 3 gives examples of the momentum transfer efficiency, calculated from (7) and (8) by numerical integration, and crater radii from (3), for a 1 m diameter spherical impactor of 300 kg, incident normally on the 160 m moon at 7.03 km/s, using the four sets of strength-dominated impact cases from Table 2, with high and low strength, non-porous and porous targets. The basalt case (high strength, zero porosity) may not be relevant to Didymos, if the binary system formed as a result of YORP spin-up and centrifugal shedding of material (Richardson and Walsh, 2006; Walsh et al., 2012). The WCB case is low porosity, and moderately high strength, but the ROSETTA comet 67P/Churyumov–Gerasimenko has an even greater strength below a shallow surface layer (Knapmeyer et al., 2014), and the WCB case might be relevant to Didymos. The other cases are low strength, moderate or high porosity cases. Both PS and SFA may be realistic target material cases for the Didymos secondary.

Table 3
DART kinetic impact results, numerical integrations.

	Basalt C2	WCB C3	PS C8	SFA C7
Momentum transfer efficiency, β	3.324	1.096	1.229	1.30
Crater radius, R (m)	4.89	3.06	8.47	5.70
With system escape speed, β^*	3.324	1.096	1.215	1.30
Temporary orbiting mass (%)	<1	<1	32	<1

With the more realistic velocity distributions, the β predictions in Table 3 for the DART impact, modeled as a 300 kg sphere at 7.03 km/s, are similar to previous results (Holsapple and Housen, 2012; Jutzi and Michel, 2014; Cheng et al., 2015), with the basalt case yielding much higher values than the other cases. The β for basalt is high because of high $C_1 k$. For the other target material cases, β is in the range 1.1–1.3. The predicted β from the DART impact is uncertain and could span at least the range of values shown in Table 3.

The calculations of β and R in Table 3 use a moon radius of 80 m and its escape velocity ignoring the primary (assuming the moon to be a single body), $v_{esc} = 9.2$ cm/s. The calculation of β^* in Table 3 was performed in the same way, except that the value of the escape velocity was increased to that for the binary system $v_{esc}{}^* = 24.4$ cm/s for ejecta released at 1.18 km from the system barycenter. By comparing the values of β and β^*, we may estimate the effect of the gravity well of the primary on the result of the kinetic impact experiment. The idea is that β includes the momentum contributions from all ejecta faster than v_{esc}, whereas β^* includes only contributions from ejecta faster than $v_{esc}{}^*$ that are able to escape from the binary system. Table 3 shows that the values of β and β^* are quite similar, indicating that only a small contribution to the momentum transfer comes from ejecta which are released just above the escape velocity but below the binary system escape velocity. Ejecta released from the moon above v_{esc} but below $v_{esc}{}^*$ are trapped into temporary binary orbits, to be accreted by the primary, re-accreted by the secondary, or eventually lost from the system. The fate of the temporarily orbiting ejecta will be the subject of future studies.

Table 3 shows that the momentum transfer efficiency β is only slightly affected by the presence of the Didymos primary, whose gravitation causes very slow ejecta to be captured into transient binary orbits after escaping from the secondary. The main result of the DART deflection experiment, measurement of β from the impact on the Didymos secondary, is only slightly affected by targeting the secondary of a binary system. For three of the target material cases (basalt, WCB, SFA), the value of β is not affected to 3 significant figures by including only ejecta above the Didymos system escape velocity. In the other case PS, the most porous and lowest strength case, the reduction in β by 0.01 may be within experimental uncertainties. Table 3 gives three or four significant figures in order to make the comparison between β and β^*. Jutzi and Michel (2014) have previously found that ejecta just above the escape velocity, from a homogeneous microporous target, make only a small contribution to the momentum transfer.

For the PS case, Table 3 shows that 32% of the ejecta mass will be captured into temporary binary orbits. These ejecta were launched at low velocity and hence made little contribution to β.

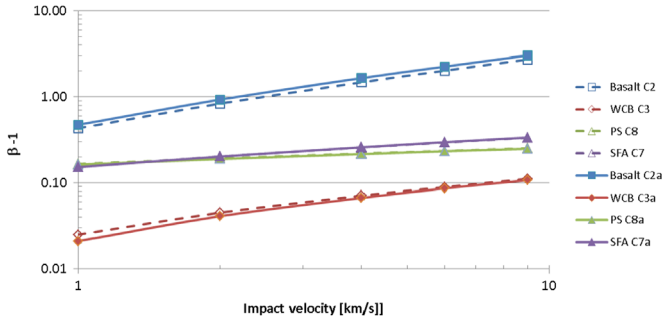

Fig. 4. Momentum transfer, impact of 300 kg, 1 m diameter projectile at various velocities. From numerical integrations of (7) and (8) with dashed lines and open symbols; also from analytic approximation (9) with solid lines and filled symbols, for the four target cases in Table 2. Analytic approximation labeled with a; e.g. C2a (approximate) and C2 (numerical).

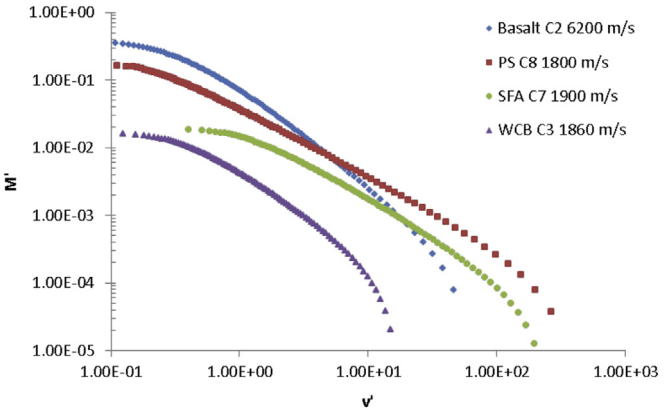

Fig. 5. Ejecta velocity distributions of Table 2 in dimensionless strength-scaled form, with the four cases labeled by impact velocity.

For the other target material cases, $<1\%$ of the ejecta mass is captured into temporary orbits.

The value of β will depend on the projectile radius even for a fixed mass and impact velocity, because of dependence on the projectile density. This effect is illustrated as follows. In Table 3, the 300 kg spacecraft is assumed to be of radius 0.5 m (approximately matching the mass per unit cross-section area) giving $\beta = 3.32$, but if the projectile is assumed to be radius 0.28 m, giving it a basalt-like density 3263 kg m^{-3} with all else staying the same, then β is increased to 4.56. The increase in β at higher projectile density is most pronounced for the basalt C2 case. In the PS C8 case, the same increase in projectile density results in $\beta = 1.40$ compared to $\beta = 1.229$ as shown in Table 3.

Fig. 4 compares the approximation (9) to the numerical integrations of (7) and (8), assuming DART-like kinetic impacts of a 300 kg, 1 m diameter sphere over a range of impact velocities. Fig. 4 shows $\beta - 1$ versus incident velocity for the four target material cases. The numerically integrated $\beta - 1$ values over the four cases use the ejecta velocity distributions fitted to experimental data (Housen and Holsapple, 2011) and do not have power law dependences on incident velocity. The approximation (9) as used in Fig. 4 includes the n_1 term, so that $\beta - 1$ is still not a power law in impact velocity. The analytic approximation (9) is within $\sim 11\%$ of the numerical result in the worst cases (basalt C2 and WCB C3), and it is within $\sim 1\%$ for the porous cases (PS C8 and SFA C7).

The results for β shown in Table 3 and Fig. 4 are in excellent agreement (for the cases other than basalt) with the results of Smoothed Particle Hydrodynamics (SPH) code simulations with a porous material equations of state fitted to laboratory crush-curve data (Jutzi and Michel, 2014). The ejecta velocity distributions, or mass M ejected at velocity $> v$, are appropriately expressed in terms of dimensionless strength parameters (Holsapple and Housen, 2012)

$$M' = \frac{M}{m}\left(\frac{U}{\sqrt{Y/\rho}}\right)^{-3\mu}\left(\frac{\rho}{\delta}\right)^{3\nu-1}$$

$$v' = \frac{v}{\sqrt{Y/\rho}}$$

There are typographical errors in Figure 15 (vertical axis label) of Holsapple and Housen (2012) and Figure 3 (caption) of Jutzi and Michel (2014). Fig. 5 shows the ejecta velocity distributions of Table 2, which were used to find β in Table 3 and Fig. 4, when expressed in the dimensionless strength parameters.

The $M'(v')$ distributions in Fig. 5, which were fitted to experimental data (Housen and Holsapple, 2011), display approximate power law regions with slope $M' \propto (v')^{-3\mu}$, where the slope is steepest for the non-porous basalt C2 case and becomes less steep as the porosity increases, as indicated by the μ values in Table 2. Similar values of μ are found for basalt C2 and for WCB C3, although the former was measured at 6.2 km/s and the latter was measured at 1.86 km/s. Both fairly high and low μ values are found in the three porous target cases of Table 2, all of which were measured between 1.8 and 1.9 km/s. The $M'(v')$ distributions in Fig. 5 are similar to those found by SPH code calculations (Jutzi and Michel, 2014), where a case is reported with a high $\mu \sim 0.6$ at 1 km/s impact velocity and cases with low $\mu \sim 0.4$ are reported with impact velocities ≥ 5 km/s.

Table 4
SPH simulation results (Jutzi and Michel, 2014) showing projectile density, porosity, and shape effects.

δ (kg/m^3)	Shape	Projectile porosity (%)	β
100	Spherical	0	1.5
100	Spherical	95	1.8
1000	Spherical	0	2.5
1000	Circular plate	0	2.0
3000	Spherical	0	2.8

The Smoothed Particle Hydrodynamics (SPH) impact simulation code of Jutzi and Michel (2014) was used in the context of the NEOShield project funded by the European Commission to explore the influences of projectile density and porosity as well as projectile shape at constant projectile mass (Table 4). These simulations used a Tillotson equation of state and a Drucker–Prager yield criterion with shear strength depending on the confining pressure. The three spherical projectile cases at 0% porosity explore the effect of projectile density δ. A comparison is also made at density $\delta = 100$ kg/m^3 between a non-porous and a porous projectile that has a pumice crush-curve equation of state (Jutzi et al. 2009). Finally the two cases at $\delta = 1000$ kg/m^3 compare different projectile shapes, where the sphere is compared to a thin plate with 3 times greater radius at the same mass. All of these cases assumed the same target material, with pumice crush-curve parameters for 10% porosity and 2400 kg/m^3 density, and all use the same target diameter of 300 m. The impact velocity was 10 km/s in all cases.

The three cases of non-porous spherical projectile in Table 4 give an approximate power law dependence of $\beta - 1$ on projectile density, with an exponent on the density of 0.39, slightly different from the value of 0.2 found by Holsapple and Housen (2012, their Eq. (36)). The scaling laws predict (e.g., Eq. (10)) that the exponent on the density is $3\nu - 1$, which is 0.2 for $\nu = 0.4$ as in Table 2. The exponent of 0.39 results in a value of $\nu = 0.46$, which is not very different from the experimental value.

The projectile porosity and shape dependences are also exhibited in Table 4. The highly porous spherical projectile has an increased β compared to that for the non-porous sphere, whereas the flat circular plate yields a lower β than the much more compact spherical projectile. Even with the extreme projectile porosity difference and shape difference considered in Table 4, the resulting differences in β are similar to the effects of different target materials (Table 3).

If the point of view is adopted that the scaling law model (3–7) is simply an empirical model with adjustable parameters to fit experimental results, then it may be possible to account for projectile structure effects. For example, the projectile shape comparison at $\delta = 1000$ kg/m^3 can be reproduced by changing the basalt C2 case as follows: match target diameter and impact velocity; use $C_1 = 0.6$; adjust n_1 to account for shape difference. Then for the sphere, $\beta = 2.4$ at $n_1 = 1.2$, while for the thin plate $\beta = 2.0$ at $n_1 = 4.1$, an increase in n_1 similar to the increase in radius from sphere to thin plate.

4.3. Dust and ejecta distributions

The result of the DART kinetic impact will be not only to make a crater of ~6 to ~17 m diameter (Table 3) but also to release a large volume of particulate ejecta that may be directly observable from Earth or even resolvable as a coma or an ejecta tail by ground-based telescopes. The ejecta cloud released by the DART impact on Didymos will increase the amount of reflected sunlight in proportion to the cross sectional area of ejecta compared to that of Didymos, assuming ejecta to have the same albedo. The ejecta area is estimated assuming a size distribution adopted from the size distribution measured for Itokawa regolith (gravel, cobbles and blocks) by Hayabusa (Miyamoto et al., 2007), which gives the cumulative number N of regolith pieces larger than a diameter d in meters as $N(>d) = 4.8e4d^{-2.8}$. The corresponding differential size distribution is $n(d) = 1.344e5d^{-3.8}$. This assumed regolith size distribution is not meant to indicate an expectation that the collisional evolution of Didymos is the same that of Itokawa. The size distribution may result from impact processing and/or from additional processes such as fracturing from thermal fatigue (Michel et al., 2015b).

From this size distribution we find the total cross sectional area of regolith pieces A_d in the size range d_1 to d_2 as $A_d = \int_{d_1}^{d_2} ds\pi s^2 n(s)$. Similarly we find the total volume of regolith pieces in the same size range, $V_d = \int_{d_1}^{d_2} ds((\pi s^3)/6)n(s)$. Then we form the area-to-mass ratio of the regolith using the target density ρ, adopting a size range $d_1 = 1$ mm to $d_2 = 10$ cm. We obtain the released ejecta mass M from integration of (6) and then obtain the released cross sectional area $\frac{MA_d}{\rho V_d}$. This area is compared with that of Didymos itself, to estimate first the increase in brightness from the increase in cross sectional area caused by ejecta release, and then the integrated brightness of the ejecta considered as a coma. The results are shown in Table 5 for the four target material and impact cases of Table 2. The ejecta coma may be observable with Earth-based telescopes.

Table 5
Brightness of coma from ejecta released by DART kinetic impact.

	Basalt C2	WCB C3	PS C8	SFA C7
Didymos brightening (mag)	−0.08	−0.02	−0.38	−0.12
Coma, integrated V mag	17.3	18.8	15.5	16.8

4.4. Catastrophic disruption

As the primary objective of the DART mission is to perform a full-scale demonstration of asteroid deflection by kinetic impact, the scale of the impact should be far below the threshold for catastrophic disruption, where the mass of the largest remnant after the impact has only half the original mass of the target. That the DART impact is far from the catastrophic disruption threshold can be inferred from the predicted crater radii shown in Table 3, where in all four cases the crater radius R is much smaller than the target body radius of 80 m. In addition, the specific energy of the DART impact (kinetic energy of impact divided by target mass) is small compared to the critical specific energy Q_D^* that leads to catastrophic disruption. The results of numerical simulations (Jutzi et al., 2010) of impacts at 5 km/s into porous and non-porous targets are fitted by the sum of two power laws

$$Q_D^* = Q_0 {R_p}^a + B\rho {R_p}^b$$

where R_p is the target body radius and the constant coefficients Q_O, B,a,b are given in Table 3 of Jutzi et al. (2010). The DART specific energy Q^* is 1.47×10^4 erg/g, whereas the catastrophic disruption thresholds in this model are found to be $Q_D^* = 2.53 \times 10^6$ erg/g (porous); $Q_D^* = 1.63 \times 10^6$ erg/g (non-porous).

5. Discussion and conclusions

The AIDA mission will combine US and European space experience and expertize to address an international concern, the asteroid impact hazard. AIDA will target the binary near-Earth asteroid Didymos with two independently launched spacecraft, with the DART kinetic impact experiment to occur in late September or October, 2022. DART will return fundamental new information on the response to impact of an asteroid as a function of its strength, surface physical properties, and internal structure, and it will improve and validate models and simulations of kinetic impact to reduce uncertainty of momentum transfer in future kinetic impactor missions.

The DART mission, considered as a stand-alone mission, measures the binary period change from the DART impact, which determines the kinetic energy transfer to orbital energy and allows β to be inferred. DART determines the location of the impact and obtains high-resolution images of the impact site. Together with the AIM rendezvous mission, the β factor of the DART impact is measured directly from characterizing the binary orbit before and after the impact. AIM also characterizes the target body before and after the DART impact, determining physical properties such as density and porosity.

The combined information from DART and AIM yields inferences on the responses of the asteroid target to the kinetic impact. AIDA will thus be the first fully documented impact experiment at asteroid scale. Although the β values in Table 3 are rather similar for the porous target cases (WCB, PS, SFA), and similar to those predicted for porous targets by numerical simulations (Jutzi and Michel, 2014), the predicted crater radii R are quite different in the different cases. The AIM determination of crater radius R is important for sorting out target material properties. A much greater mass is ejected for the PS case than for SFA, but the β is not very different because the ejecta are much slower for PS. The ejecta mass is also determined directly by AIM from crater observations and from imaging of ejecta, while telescopic observations supported by the DART mission may also be able to monitor the dynamics and evolution of an ejecta coma.

Acknowledgments

We thank the engineering teams at APL and ESTEC-CDF for valuable discussions. We thank NASA for support of the DART study under Contract/task numbers NNN-06AA01C and NNN-13AA12T. Numerical simulations of projectile shape and density effects on momentum transfer were performed under the NEOShield project funded by the EU FP7 program Agreement no. 282703. PM acknowledges support from the European Space Agency.

References

A'Hearn, M.F., et al., 2005. Deep impact: excavating comet tempel 1. Science 310, 258–264.

Ahrens, T.J., Harris, A.W., 1994. Deflection and fragmentation of near-Earth Asteroids. In: Hazards due to Comets & Asteroids. University of Arizona Press, pp. 897–927.

Brown, P.G., et al., 2013. A 500-kiloton airburst over Chelyabinsk and an enhanced hazard from small impactors. Nature 503, 238–241.

Carnelli, I., Galvez, A., Ongaro, F., 2006. Learning to deflect near-Earth objects: industrial design of the Don Quijote mission. In: Proceedings of the 57th International Astronautical Congress, Valencia, Spain. doi: 10.2514/6.IAC-06-A3.5.05.

Cheng, A.F., et al., 2008. Long-range reconnaissance imager on new horizons. Space Sci. Rev. 140, 189. http://dx.doi.org/10.1007/s11214-007-9271-6.

Cheng, A.F., et al., 2015. Asteroid impact and deflection assessment mission. Acta Astronaut. 115, 262–269. http://dx.doi.org/10.1016/j.actaastro.2015.05.021.

Cheng, A.F., 2013. AIDA: test of asteroid deflection by spacecraft impact. In: Proceedings of the 44th LPSC 2013, Paper 2985.

Cintala, M.J., Berthoud, L., Hörz, F., 1999. Ejection-velocity distributions from impacts into coarse-grained sand. Meteorit. Planet. Sci. 34, 605–623.

Gault, D.E., Wedekind, J.A., 1978. Experimental studies of oblique impact. Lunar Planet. Sci. Conf. 9 3843–3843–3875–3875.

Harris, A.W., et al., 2013. The European Union funded NEOShield Project: a global approach to near-Earth object impact threat mitigation. Acta Astronaut. 90, 80–84.

Holdren, J., 2010. Letter to Congress ⟨https://www.whitehouse.gov/sites/default/files/microsites/ostp/ostp-letter-neo-senate.pdf⟩.

Holsapple, K.A., Housen, K.R., 2012. Momentum transfer in asteroid impacts. I. Theory and scaling. Icarus 221, 875–887.

Housen, K., Holsapple, K., 2011. Ejecta from impact craters. Icarus 211, 856–875.

Jutzi, M., Michel, P., 2014. Hypervelocity impacts on asteroids and momentum transfer. I. Numerical simulations using porous targets. Icarus 229, 247–253.

Jutzi, M., Michel, P., Hiraoka, K., Nakamura, A., Benz, W., 2009. Numerical simulations of impacts involving porous bodies II. Comparison with laboratory experiments. Icarus 201, 802–813.

Jutzi, M., Michel, P., Benz, W., Richardson, D.C., 2010. Fragment properties at the catastrophic disruption threshold: the effect of the parent body's internal structure. Icarus 207, 54–65.

Knapmeyer, M. et al., 2014. Mechanical Properties of the Surface Material of Comet 67P/Churyumov–Gerasimenko Measured By the Case Instrument Onboard the Philae Lander, AGU Fall Meeting, Abstract no. P34B-04.

Margot, J.L., et al., 2002. Binary asteroids in the near-Earth object population. Science 296, 1445–1448.

Michel, P., 2013. Physical properties of near-Earth objects that inform mitigation. Acta Astronaut. 90, 6–13.

Michel, P., et al., 2015a. Asteroid Impact Mission: Didymos Reference Model. AIM Phase A/B1, ESA.

Michel, P., et al., 2015b. Temperature shocks at the origin of regolith on asteroids. Highlights Astron. 16, 162.

Michel, P., et al., 2016. Science case for the Asteroid Impact Mission (AIM): a component of the Asteroid Impact & Deflection Assessment (AIDA) Mission. Adv. Space Res. (submitted for publication)

Miyamoto, H., et al., 2007. Regolith migration and sorting on asteroid Itokawa. Science 316, 1011–1014.

Popova, O.P., et al., 2013. Chelyabinsk airburst, damage assessment, meteorite recovery, and characterization. Science 342, 1069–1073.

Pravec, P., et al., 2003. (65803) 1996 GT, IAU Circular 8244.

Pravec, P., et al., 2006. Photometric survey of binary near-Earth asteroids. Icarus 181, 63–93.

Richardson, D., Walsh, K., 2006. Binary minor planets. Ann. Rev. Earth Planet. Sci. 34, 47–81.

Scheirich, P., Pravec, P., 2009. Modeling of light curves of binary asteroids. Icarus 200, 531–547.

Walsh, K.J., Richardson, D.C., Michel, P., 2012. Spin up of rubble pile asteroids: disruption, satellite formation, and equilibrium shapes. Icarus 220, 514–529.

Yamamoto, S., Barnouin-Jha, O.S., Toriumi, T., Sugita, S., Matsui, T., 2009. An empirical model for transient crater growth in granular targets based on direct observations. Icarus 203 (1), 310–319. http://dx.doi.org/10.1016/j.icarus.2009.04.019.